First-principles investigation of strain effects on the energy gaps in silicon nanoclusters

2007 J. Phys.: Condens. Matter 19 266212

(http://iopscience.iop.org/0953-8984/19/26/266212)

IOP PUBLISHING JOURNAL OF PHYSICS: CONDENSED MATTER

J. Phys.: Condens. Matter **19** (2007) 266212 (9pp) doi:10.1088/0953-8984/19/26/266212

First-principles investigation of strain effects on the energy gaps in silicon nanoclusters

X-H Peng[1,2], A Alizadeh[1], N Bhate[1], K K Varanasi[1], S K Kumar[3] and S K Nayak[2]

[1] General Electric Global Research Center, Niskayuna, NY 12309, USA
[2] Department of Physics, Applied Physics and Astronomy, Rensselaer Polytechnic Institute, Troy, NY 12180, USA
[3] Department of Chemical Engineering, Columbia University, New York, NY 10027, USA

E-mail: pengx@rpi.edu

Received 23 February 2007, in final form 23 May 2007
Published 14 June 2007
Online at stacks.iop.org/JPhysCM/19/266212

Abstract

First-principles density functional calculations were performed to study strain effects on the energy gaps in silicon nanoclusters with diameter ranging from 0.6 to 2 nm. Hydrostatic and non-hydrostatic strains have been found to affect the energy gaps differently. For the same strain energy density, non-hydrostatic strain leads to a significantly larger change in the energy gap of silicon clusters compared to that of the hydrostatic strain case. In contrast, hydrostatic and non-hydrostatic strain effects on the energy gaps of bulk Si or larger size Si quantum dots are comparable. Non-hydrostatic strains break the tetrahedral bonding symmetry in silicon, resulting in significant variation in the energy gaps due to the splitting of the degenerate orbitals in the clusters. Our results suggest that the combination of energy gaps and strains permits the engineering of photoluminescence in silicon nanoclusters and offers the possibility of designing novel optical devices and chemical sensors.

1. Introduction

The research area of nanoscale semiconductor structures has attracted considerable attention over the past two decades. It has been shown that below a critical size (e.g. the exciton Bohr radius of the bulk material), nanoscale semiconductors tend to exhibit unusual properties primarily due to quantum confinement effects. For example, the band gap (or energy gap) in a semiconductor nanocrystal increases significantly with the reduction in crystal size [1–6]. The occurrence of such unusual properties has created a plethora of opportunities and applications that exploit semiconductor nanostructures. For instance, the size of semiconductor nanostructures in the active region of luminescent devices can be tuned to control their emitting wavelength. Indeed, the size effect on the energy gap (EG) in direct gap semiconductors

(e.g. CdSe, PbS, PbSe) has been exploited in a wide range of applications, such as solar cells, light emitting diodes (LEDs), electroluminescence, optoelectronics, photonics, security ink, and biotags [7–10]. Silicon has been the mainstay material for electronics, but had a limited impact on the area of optoelectronics because of its indirect band gap, low electron mobility, and its inability to exhibit the electro-optic Pockels effect. However, recent breakthroughs such as doping Si with erbium to overcome the indirect band gap [11], optical amplification through Raman effect [12], dislocation engineering [13, 14], fast Si optical modulator [15], and Raman Si laser [16–18] have sparked intense interest in the field of bulk Si photonics [19, 20]. These advances dramatically change the fortunes of Si as a material for optoelectronic applications. In this field, nanostructured Si occupies a distinctive place, since it exhibits visible photoluminescence unlike its bulk counterpart. The phenomenon of visible photoluminescence in Si was first discovered by Canham [21] in the early 1990s. Since then several researchers have conducted experimental and theoretical studies showing that EG in Si nanoclusters can be modified by varying their dimensions and/or their surface composition [1–3, 22–25]. In the semiconductor industry, band gaps of bulk semiconductors are routinely engineered by applying strain and corresponding deformation potentials. Liao *et al* [26] investigated the effect of biaxial tensile mechanical strain on the metal–oxide–silicon light emitting diode and found that EG in Si decreases continuously under strain. Buda *et al* [27] studied EG in the III–V semiconductor clusters encapsulated in a sodalite cage and observed a shift in EG due to the resultant tensile/compressive strain exerted by the cage.

In our previous study [28], the effect of hydrostatic strain on EG in Si nanoclusters was reported. We found that strain effects on the band gaps display qualitatively new trends for nanoclusters smaller than 2 nm. While the bulk indirect band gap increases linearly with increasing strain, this trend is reversed in small clusters less than 1 nm. In the intermediate size range of 1–2 nm, hydrostatic strain appears to have almost no effect. Finally, for clusters larger than 2 nm, the bulk behaviour is recovered. In the present work, we extend our previous investigation to include other types of strain that result in bond angle distortion in Si nanoclusters. In particular, we focus on two types of non-hydrostatic strains, namely biaxial and shear.

2. Methodology

The electronic properties of a series of Si clusters are carried out using first-principles density functional theory (DFT) based on the generalized gradient approximation (GGA) [29]. In particular, we have used Perdew–Wang 91 (PW91) exchange and correlation functional [30] and pseudopotential plane wave approach with the supercell method. The core electrons are described using ultrasoft Vanderbilt pseudopotentials [31] within the computational VASP code [32]. The size of the simulation cell is chosen so that the distance between the cluster and its replica (due to the periodic boundary condition) is more than 1.2 nm. Under this configuration, the interactions between the cluster and its replica are negligible. The kinetic energy cut-off for the plane wave basis set is 300 eV corresponding to about 10^6 plane waves in the cubic simulation cell (3 nm in side). We used 600 eV cut-off for the convergence test on a small cluster Si_5H_{12} and found that the change in EG is less than 0.02%.

Spherical Si clusters in the size range of 0.6–2 nm, with one Si atom at the centre, are used in this study. The original coordinates of the clusters are derived from bulk Si with a lattice constant of 0.5461 nm. The dangling bonds on the surface are passivated using hydrogen atoms to maintain the tetrahedral configuration in Si, at an initial Si–H bond length of 0.147 nm. The clusters are then relaxed to minimize the total energy using the conjugate gradient algorithm. The local minimum is achieved when all the residual forces acting on the atoms are less than

0.02 eV Å^{-1}. We also used a more stringent relaxation criterion of 0.002 eV Å^{-1} and found that it has a negligible effect (less than 0.1%) on EG.

EG in Si nanocluster is defined as the energy difference between the highest occupied molecular orbital (HOMO, i.e. valence band) and lowest unoccupied molecular orbital (LUMO, i.e. conduction band). It is known that density functional method underestimates the band gap as compared to the experimental value, while the more accurate GW method [33] and Monte Carlo calculations provide better quantitative predictions. However, previous studies on Si nanoclusters and nanowires show that the HOMO–LUMO gap predicts a similar size dependence to the optical gap obtained by the GW and quantum Monte Carlo methods [24, 34]. In addition, as reported by Peng *et al* [28], the variation of HOMO–LUMO gap with hydrostatic strain is in excellent agreement with that of the optical gap predicted from the advanced configuration interaction method. Based on this information we anticipate our results would correctly describe the strain effects on EG in Si clusters.

The delineations of the biaxial and shear strains, as well as the hydrostatic strain for the purpose of later comparison, are given in the following. Hydrostatic strain is applied to the cluster by rescaling the three coordinates of all the atoms up to $\pm 8\%$. Positive strain refers to expansion of a cluster while negative strain corresponds to its compression. In the case of biaxial strain, the nanocluster is deformed in two dimensions while the unconstrained third dimension is allowed to accommodate the resulting deformation. In a typical simulation, we apply two-dimensional in-plane strains of up to $\pm 8\%$ by rescaling x and y coordinates of the atoms followed by relaxing the entire structure. In contrast to the hydrostatic strain, which only modifies the bond lengths homogeneously, the biaxial strain results in a change in the bond angle. This angle change leads to a distortion of Si tetrahedral bonding network. The other non-hydrostatic type of strain we considered is shear strain. It should be noted the definition of shear at nanoscale is not unique, and the continuum mechanics community has identified the plethora of issues related to the so-called Cauchy–Born rule for non-standard shaped nanosized clusters [35]. In this paper, simple shear strain is mathematically defined as $\tan\theta = \Delta d/l$, where l is the original length of a given line, Δd is the amount of deformation perpendicular to that given line, and θ is the angle the sheared line makes with its original orientation. In our study on shear strain, l is taken as the z coordinate of the atoms and Δd is the displacement of the atoms along x-direction. Similar to the case of the biaxial strain, the shear strain results in a distortion of the Si tetrahedral bonds. We realize that the magnitudes of the strains are beyond the elastic limit in bulk Si. However, in the case of nanoclusters, the nucleation of defects, such as dislocations and disclinations, remains energetically unfavourable until the strain reaches a considerably higher level [36].

3. Results and discussion

A series of Si clusters with one atom at the centre are studied in present work. The characteristics of these clusters are summarized in table 1. The diameter of a given cluster is determined by the formula $a(0.75N_{\mathrm{Si}}/\pi)^{1/3}$, where N_{Si} and a are the number of Si atoms and the lattice constant (0.5461 nm), respectively. EG in the last column is the HOMO–LUMO gap of the geometry-relaxed cluster calculated using DFT (PW91). Our predicted energy gaps for Si clusters are in excellent agreement with previous studies [1, 3, 23] and a detailed comparison between our results and the literature is presented in [28].

Subsequently, biaxial and shear strains are applied to the clusters. The effect of biaxial strain on EG in Si clusters and bulk is shown in figure 1. As seen in the figure, EG decreases, almost in a parabolic fashion, under both tensile (positive sign) and compressive (negative sign) strains in all cases. For example, EG in $Si_{35}H_{36}$ is decreasing from 3.51 to 3.24 eV for

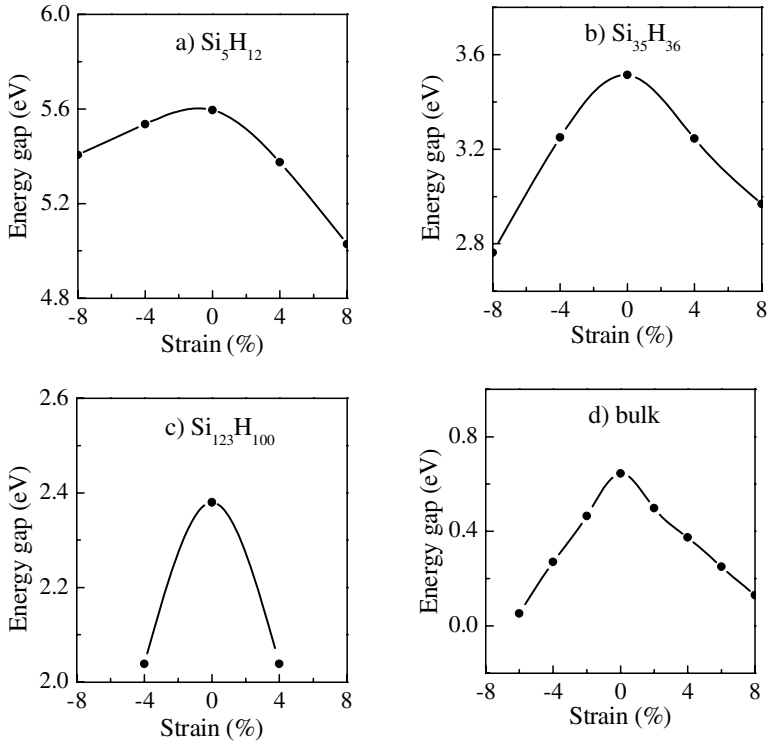

Figure 1. The DFT HOMO–LUMO gap as a function of biaxial strain for different size Si clusters and bulk, (a) Si_5H_{12}; (b) $Si_{35}H_{36}$; (c) $Si_{123}H_{100}$; (d) bulk. Positive strain refers to expansion while negative strain corresponds to compression.

Table 1. A list of studied Si clusters in present work. N_{Si} is the number of Si atoms in a given cluster; N_H is the number of H atoms needed to saturate the surface dangling bonds. The columns of x coordination (for short, 'x-coord.', $x = 1, 2, 3, 4$) represent the numbers of Si atoms which connect to other x Si and have $4 - x$ dangling bonds. The diameter of a cluster is determined by the number of the Si atoms through the formula $a(0.75N_{Si}/\pi)^{1/3}$ where a is Si lattice constant 0.5461 nm. EG is the DFT HOMO–LUMO gap for the geometry-relaxed cluster.

N_{Si}	N_H	4-coord.	3-coord.	2-coord.	1-coord.	Diameter (nm)	EG (eV)
5	12	1	0	0	4	0.58	5.60
17	36	5	0	0	12	0.87	4.28
29	36	5	12	12	0	1.04	3.64
35	36	5	24	6	0	1.11	3.51
47	60	17	12	6	12	1.22	3.20
59	60	17	24	18	0	1.32	3.00
87	76	35	28	24	0	1.50	2.59
123	100	59	28	36	0	1.68	2.38

both tensile and compressive 4% biaxial strains. Similarly, EG in $Si_{123}H_{100}$ decreases from 2.38 to 2.04 eV under ±4% strain. In order to understand the EG–strain relation presented in figure 1, we further examined the energies of HOMO and LUMO in these clusters. We found the HOMO energy to vary with the biaxial strain in a similar fashion for all the clusters listed in table 1. Specifically, the HOMO energy increases with both tensile and compressive biaxial

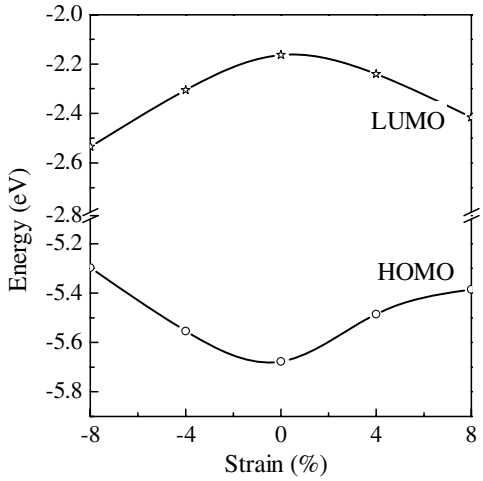

Figure 2. The variation of the orbital energies of HOMO and LUMO in $Si_{35}H_{36}$ under biaxial strain.

strain. Meanwhile, the LUMO energy decreases under biaxial expansion and compression. As an example, the LUMO and HOMO energies in the cluster $Si_{35}H_{36}$ as a function of biaxial strain are presented in figure 2. We will continue to use this cluster $Si_{35}H_{36}$ as a study case in the remainder of the paper for understanding of various properties. Figure 2 shows that the LUMO energy decreases while the HOMO energy increases with biaxial strain. We will discuss the possible reasons for the energy variations of LUMO and HOMO in Si clusters in greater detail later in the paper.

In the case of shear strain, we applied deformation along positive x-direction. As in case of biaxial strain, the variation in EG with shear strain is independent of the cluster size. For all clusters listed in table 1, the decrease in EG with shear strain is similar to that of bulk Si. EG, HOMO and LUMO energies as a function of shear strain for the cluster $Si_{35}H_{36}$ are shown in figure 3. As can be seen in this figure, both EG and LUMO energy decrease dramatically with shear strain, whereas the HOMO energy increases more gradually with strain.

In brief, biaxial and shear strains result in reduced EG in Si clusters. In order to explain the observed variations of EG, HOMO and LUMO energies with strain, we have examined the molecular orbitals of the Si clusters near their Fermi level. The orbital energies near the Fermi level in the cluster $Si_{35}H_{36}$ (relaxed and under strains) are presented in figure 4. L2, L5 and L7 are the energy levels in the unstrained relaxed $Si_{35}H_{36}$; L1 and L3 are the energy levels in $Si_{35}H_{36}$ under hydrostatic compression and expansion; L4 and L6 display orbital levels under biaxial compression and expansion; while L8 shows orbital energies under shear strain. The Fermi level is represented by the dotted line in the middle. For the relaxed cluster, the molecular orbitals typically degenerate due to the tetrahedral symmetry in Si. The degeneracy of an orbital is represented by the number of dashes in a line in figure 4. For instance, HOMO in relaxed $Si_{35}H_{36}$ (see L2) is a threefold degeneracy and it is described by a line with three dashes. As mentioned in the earlier section, hydrostatic strain is isotropically applied to the cluster and only changes the length of the bonds, without affecting the bond angles i.e. the tetrahedral symmetry in the Si network is preserved under the hydrostatic strain. As a result, the hydrostatic strain does not split the degenerate orbitals as seen in L1 and L3 in figure 4. For instance, the threefold degeneracy of HOMO in L2 is preserved under hydrostatic strain. The energy shifts

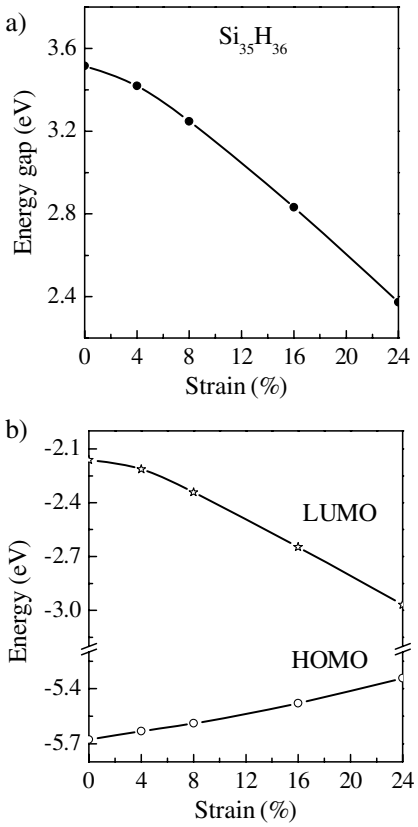

Figure 3. (a) The energy gap in $Si_{35}H_{36}$ as a function of shear strain; (b) the variation of the orbital energies of HOMO and LUMO in $Si_{35}H_{36}$ with the shear strain.

of HOMO and LUMO under hydrostatic strain in this size range can be understood from their orbital characters as follows (see [28]). Both HOMO and LUMO of the cluster have bonding characters (not shown here), that is, the electron cloud is mainly located in the intermediate regions shared by silicon atoms. The reduction of Si–Si bond lengths on compression make the electron cloud of HOMO and LUMO more efficiently shared by Si atoms. This results in an increased electron–nucleus Coulomb attraction, thus an appreciable decrease of both HOMO and LUMO energy levels (the change in the electron–electron repulsion energy is relatively small). In contrast, with expansion, both HOMO and LUMO energy levels increase due to the decrease of electron–nucleus attraction. This results a negligible change in the EG [28]. However, the non-hydrostatic strains studied distort the clusters and break the Si tetrahedral symmetry. We expect this distortion to result in splitting of the degenerated orbitals as seen in L4, L6 and L8 in figure 4. For example, the threefold HOMO has been split into two levels under biaxial strain and into three levels under shear strain. Note that in the case of biaxial strain, the strain is applied in the xy plane by rescaling the coordinates of x, y components. The symmetry in the xy plane is still maintained thereby resulting in a twofold-degenerate state as in L4 and L6 in figure 4. Under shear strain, the symmetry in Si is largely destroyed and the degeneracy of the orbitals is lifted as shown in L8 in figure 4.

In addition to the splitting of the orbitals, we also observed shifting of the orbital energies in strained clusters. For conciseness, we will only discuss the case of shear strain, though

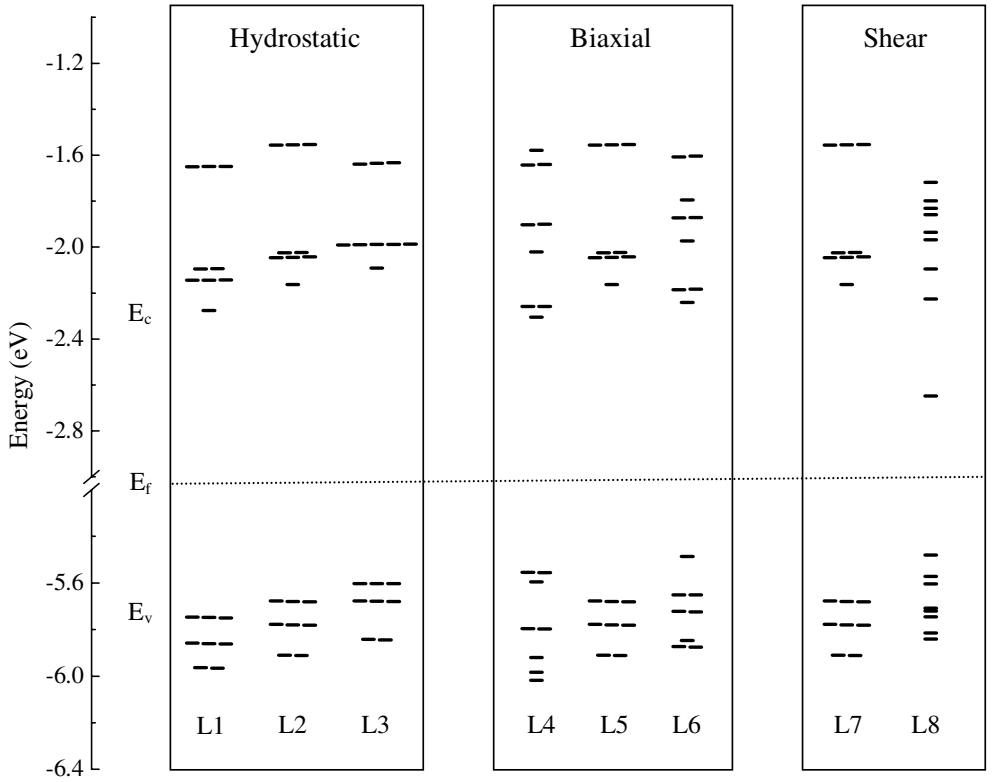

Figure 4. Orbital energies levels near Fermi level (the dotted line in the middle) in the cluster $Si_{35}H_{36}$. The degeneracy of an orbital is represented by a number of dashes in a line. L1, hydrostatic compressed; L3, hydrostatic expanded; L4, biaxial compressed; L6, biaxial expanded; L8, under shear strain; L2, L5 and L7 for the geometry-relaxed cluster and are the reference energy levels in each of the three categories of strains.

similar results are observed for clusters under biaxial strain. If we compare L7 and L8, the threefold-degenerate HOMO splits into three orbitals with different energies. The energy of the highest orbital of these three levels is now taken as the new HOMO energy. On the other hand, the LUMO energy of the strained cluster decreases because of the splitting of the degenerate orbitals above the LUMO level of the unstrained cluster.

As delineated in figure 4, hydrostatic strain modifies EG in $Si_{35}H_{36}$ negligibly because the energies of HOMO and LUMO shift down or up simultaneously under strain (see L1 and L3). However, the non-hydrostatic strains change the EG primarily because the HOMO energy increases while LUMO energy decreases under strain (see L4, L6 and L8). In addition, the absolute change in the amplitude of EG under shear strain is larger than that with biaxial strain. To gain a better understanding, we now compare the effects on EG under these three types of strains in a more quantitative manner. In figures 1–3, the variations of EG with strains are presented with strain defined as the percentages of the coordinate rescaling in Si clusters. Note that three coordinates are rescaled in hydrostatic strain; two coordinates in biaxial strain and one in shear strain. For example, under 4% strain, one expects more strain energy applied to the cluster under hydrostatic strain and less strain energy applied to the cluster under shear strain. In order to compare the clusters under equivalent deformation states in terms of strain energy, we have plotted EG as a function of strain energy density, which is defined as the difference in

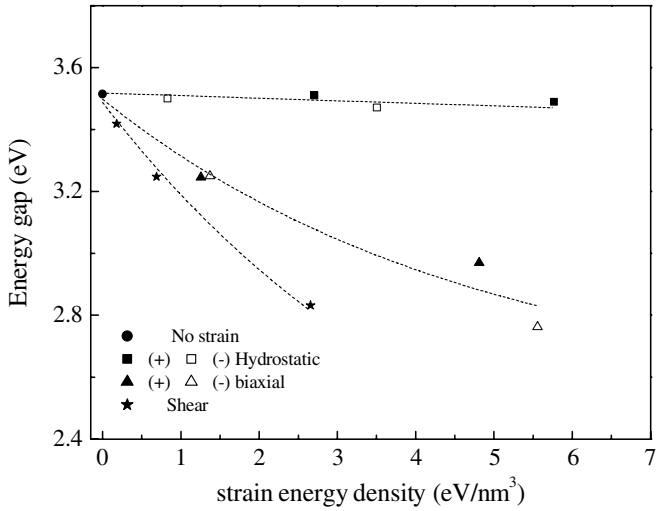

Figure 5. The energy gap in the cluster $Si_{35}H_{36}$ is expressed as a function of the strain energy density, which defined as the difference in the total energy between the strained and relaxed clusters then divided by the volume of the cluster. (●) the gap of the relaxed cluster; (■) gaps of the cluster under hydrostatic expansion; (□) gaps under hydrostatic compression; (▲) gaps under biaxial expansion; (△) gaps under biaxial compression; (★) gaps under shear strain. The dashed lines are guide for eyes.

the total energy between the relaxed and strained clusters divided by the volume of the cluster. Figure 5 shows the result of this comparison for cluster $Si_{35}H_{36}$. Clearly, hydrostatic strain exhibits a very weak influence on EG. However, biaxial strain, especially shear strain, affect EG distinctly. For instance, EG shifts down 0.04 eV with strain energy density of 3.5 eV nm^{-3} (i.e. −4% hydrostatic compression). However, EG reduces by 0.68 eV with strain energy density of 2.7 eV nm^{-3} under shear strain.

In summary, we investigated the strain effects on EG in Si nanoclusters with sizes up to 2 nm using first-principles density functional theory. We found that different types of strain affect the EG in distinct fashions. Hydrostatic strain has a relatively weak effect on EG in the size range 1–2 nm. Non-hydrostatic strains, which break the tetrahedral bonding symmetry in Si are result in significant variation in EG due to splitting of degenerate orbitals in the clusters. Our results suggest that photoluminescence in Si nanoclusters can be engineered by controlling their size and applied strain. This offers an exciting avenue for designing new classes of optical devices and chemical sensors.

Acknowledgments

This work was supported in part by NSF GOALI award no. 0327981 and the Nanotechnology Program at GE Global Research Center. We are very grateful to NCSA IBM P690 for providing the computational resources. M L Blohm, S Ganti, P Sharma, and F Tang are acknowledged for support and helpful discussions.

References

[1] Delley B and Steigmeier E F 1993 *Phys. Rev.* B **47** 1397
Delley B and Steigmeier E F 1995 *Appl. Phys. Lett.* **67** 2370

[2] Wang L-W and Zunger A 1994 *J. Chem. Phys.* **100** 2394
[3] Proot J P, Delerue C and Allan G 1992 *Appl. Phys. Lett.* **61** 1948
Delerue C, Lannoo M and Allan G 2000 *Phys. Rev. Lett.* **84** 2457
[4] Reboredo F A, Pizzagalli L and Galli G 2004 *Nano Lett.* **4** 801
[5] Peng X-H, Alizadeh A, Varanasi K K, Bhate N, Rowland L B, Kumar S K and Nayak S K 2007 First principles study of the effects of polytype and size on energy gaps in SiC nanoclusters *J. Appl. Phys.* accepted
[6] Peng X-H, Ganti S, Sharma P, Alizadeh A, Nayak S K and Kumar S K 2005 *J. Comput. Theor. Nanosci.* **2** 469
[7] Chen C C, Herhold A B, Johnson C S and Alivisatos A P 1997 *Science* **276** 398
[8] Chan W C W and Nie S 1998 *Science* **281** 2016
[9] Hirschman K D, Tsybeskov L, Duttagupta S P and Fauchet P M 1996 *Nature* **384** 338
[10] Pavesi L, Dal Negro L, Mazzoleni C, Franzo G and Priolo F 2000 *Nature* **408** 440
[11] Franzò G, Coffa S, Priolo F and Spinella C 1997 *J. Appl. Phys.* **81** 2784
[12] Claps R, Dimitropoulos D, Raghunanthan V, Han Y and Jalali B 2003 *Opt. Express* **11** 1731
[13] Ng W L, Lourenco M A, Gwilliam R M, Ledain S, Shao G and Homewood K P 2001 *Nature* **410** 192
[14] Trupke T, Zhao J, Wang A, Corkish R and Green M 2003 *Appl. Phys. Lett.* **82** 2996
[15] Liu A, Jones R, Liao L, Samara-Rubio D, Rubin D, Cohen O, Nicolaescu R and Paniccia M 2004 *Nature* **427** 615
[16] Rong H, Liu A, Jones R, Cohen O, Hak D, Nicolaescu R, Fang A and Paniccia M 2005 *Nature* **433** 292
[17] Rong H, Jones R, Liu A, Cohen O, Hak D, Fang A and Paniccia M 2005 *Nature* **433** 725
[18] Liu A, Rong H, Jones R, Cohen O, Hak D and Paniccia M 2006 *J. Lightwave Technol.* **24** 1440
[19] Reed G T and Knights A P 2004 *Silicon Photonics: An Introduction* (New York: Wiley)
[20] Pavesi L and Lockwood D L (ed) 2004 *Silicon Photonics* (Berlin: Springer)
[21] Canham L T 1990 *Appl. Phys. Lett.* **57** 1046
[22] Cullis A G and Canham L T 1991 *Nature* **353** 335
[23] Furukawa S and Miyasato T 1988 *Phys. Rev.* B **38** 5726
[24] Puzder A, Williamson A J, Grossman J C and Galli G 2002 *Phys. Rev. Lett.* **88** 097401
Puzder A, Williamson A J, Grossman J C and Galli G 2002 *Mater. Sci. Eng.* B **96** 80
Puzder A, Williamson A J, Grossman J C and Galli G 2002 *J. Chem. Phys.* **117** 6721
[25] Zhou Z-Y, Brus L and Friesner R 2003 *Nano Lett.* **3** 163
[26] Liao M H, Chen M-J, Chen T C, Wang P-L and Liu C W 2005 *Appl. Phys. Lett.* **86** 223502
[27] Buda F and Fasolino A 1999 *Phys. Rev.* B **60** 6131
[28] Peng X-H, Ganti S, Alizadeh A, Sharma P, Kumar S K and Nayak S K 2006 *Phys. Rev.* B **74** 035339
[29] Parr R G and Yang W 1989 *Density-Functional Theory of Atoms and Molecules* (Oxford: Oxford University Press)
[30] Burke K, Perdew J P and Wang Y 1998 *Electronic Density Functional Theory: Recent Progress and New Directions* ed J F Dobson, G Vignale and M P Das (New York: Plenum)
[31] Vanderbilt D 1990 *Phys. Rev.* B **41** 7892
[32] Kresse G and Furthmüller J 1996 *Phys. Rev.* B **54** 11169
Kresse G and Furthmüller J 1996 *Comput. Sci.* **6** 15
[33] Hedin L 1965 *Phys. Rev.* **139** A796
[34] Zhao X, Wei C M, Yang L and Chou M Y 2004 *Phys. Rev. Lett.* **92** 236805
[35] Yang J Z and E W 2006 *Phys. Rev.* B **74** 184110
[36] Alizadeh A, Sharma P, Ganti S, Lebouef S F and Tsakalakos L 2004 *J. Appl. Phys.* **95** 8199